



City Research Online

City, University of London Institutional Repository

Citation: Qaban, A., Mohmed, T., Quazi, M. M. & Naher, S. (2020). The effect of Al and Nb contents, cooling rate and rolling condition on the microstructure and corrosion behaviour of HSLA steel. *Materials Today Communications*, 25, 101362. doi: 10.1016/j.mtcomm.2020.101362

This is the accepted version of the paper.

This version of the publication may differ from the final published version.

Permanent repository link: <https://openaccess.city.ac.uk/id/eprint/24477/>

Link to published version: <https://doi.org/10.1016/j.mtcomm.2020.101362>

Copyright: City Research Online aims to make research outputs of City, University of London available to a wider audience. Copyright and Moral Rights remain with the author(s) and/or copyright holders. URLs from City Research Online may be freely distributed and linked to.

Reuse: Copies of full items can be used for personal research or study, educational, or not-for-profit purposes without prior permission or charge. Provided that the authors, title and full bibliographic details are credited, a hyperlink and/or URL is given for the original metadata page and the content is not changed in any way.

City Research Online:

<http://openaccess.city.ac.uk/>

publications@city.ac.uk

The effect of Al and Nb contents, cooling rate and rolling condition on the microstructure and corrosion behaviour of HSLA steel

Abdullah Qaban^{1,*}, Tasneem Mohmed¹, M.M. Quazi² and Sumsun Naher¹

¹Department of Mechanical Engineering and Aeronautics, City, University of London, London, UK

²Faculty of Mechanical and Automotive Engineering Technology, Universiti Malaysia Pahang, Pekan 26600 Pahang, Malaysia

***Corresponding Author:**

Dr. Abdullah Qaban

City, University of London

Email: Abdullah.Qaban@city.ac.uk, Abdullah_ghabban@hotmail.com

Abstract

The effect of the addition of aluminium and niobium, and processing conditions, including cooling rate and rolling condition, on the corrosion behaviour of HSLA steel in 10 wt% sulphuric acid environment has been investigated. The experimental procedures included electrochemical corrosion techniques using potentiodynamic and electrochemical impedance spectroscopy, as well as weight loss method. The microstructure was examined using optical and scanning electron microscopes in order to investigate the effect of the microstructural features on the corrosion behaviour. Surface films were evaluated by X-ray photoelectron spectroscopy (XPS) to identify the corrosion products formed on the surface. The results showed that increasing the Al content enhanced the corrosion resistance through obstructing pitting attack on the surface by the refinement of grain boundary carbides and the formation of a protective passive layer rich in carbide and oxide compounds. The combination of both Al and Nb promoted the corrosion resistance further, by enriching the passive layer with Nb and higher levels of carbide and oxide compounds, despite the presence of martensite and grain size refinement by niobium carbonitride (NbCN). Increasing the cooling rate reduced the corrosion resistance due to the refinement of grain size, giving a higher density of grain boundaries that act as active sites, besides increasing the level of carbide distribution in the microstructure. Controlled rolling offered higher corrosion resistance than hot rolling, independent of the composition, because of the absence of martensite, the presence of low-angle boundary and the refinement of grain boundary carbides provided by controlled rolling.

1. Introduction

High-strength low-alloy (HSLA) steels are widely used across many industries due to their high strength-to-weight ratio and good ductility, accompanied by the low production cost. This primary improvement in mechanical properties makes them widely suitable in many areas [1]. For instance, in the production of automotive structural components for chassis and suspension systems, in the construction industry such as bridges, and in flue gas desulfurization (FGD) systems [2]. However, due to the surrounding environment, they are highly susceptible to corrosion, ultimately reducing the lifecycle of the product. Employment of FGD systems, to battle the contribution of air pollution caused by products such as sulphur dioxide, heavily rely on highly-resistance and highly-alloyed construction materials [3,4], although, it is vital to investigate material choices that are both low in cost yet competitive, whilst maintaining the mechanical integrity. Moreover, there is evidence that corrosion can affect the mechanical

properties of steel and encourage the formation of defects [5]. These defects increase the stress concentrations and thus lead to fatigue crack initiation and accelerated corrosion [6]. Welded steel plates exposed to corrosive environments are more susceptible to stress corrosion in acidic mediums leading to severe cracking and hence causes the deterioration of tensile and flexural strength [7]. Projections indicate that global demand for sulphuric acid will continue to experience rapid growth, however, its production and use require careful design and materials selection [3].

The current authors [8] reported that adding 0.16%Al to HSLA steels enhances toughness considerably without impairing strength. A further study [9] revealed that the addition of 0.018%Nb is beneficial to improve the strength through grain size refinement and precipitation hardening [10,11]. Moreover, mechanical properties are affected by the processing conditions including the rolling condition that has a marked effect on properties, in which controlled rolling is known to further increase strength and toughness in comparison with hot rolling, but the effect of cooling rate after rolling must be taken care of [12]. Whilst studies in mechanical properties are extensive, the impact of alloying and heat treatment on corrosion resistance due to microstructural changes in acidic environments remains relatively sparse. Nb is known to encourage carbide formation at grain boundaries, while Al is effective in refining carbide thickness [13]. In addition, Nb reduces the A_{r3} temperature, the temperature at which austenite begins to transform to ferrite during cooling, so encouraging martensite formation, while Al increases the A_{r3} temperature which suppresses martensite formation, so both elements have a contradictory influence on the microstructure [8]. Moreover, identifying the best heat treatment during processing has been studied to compensate for the low alloying composition, to obtain the optimum microstructure and to achieve the desired corrosion behaviour. The most effective processing parameters on microstructural features are the type of rolling, hot and controlled rolling, and the cooling rate after rolling. Controlled rolling contributes to refining the carbides, as well as giving a finer grain size [9]. Increasing the cooling rate gives a marked refinement of grain size as well as promoting the formation of lower transformation products such as martensite [9]. These factors can have varying degrees of influence on corrosion rates; in the case of steel, studies can be contradictory and thus, the consensus remains inconclusive.

The key concept of the current work emerges as a continuation of our research on the effect of Al, Nb and their combination along with variation in the cooling and rolling conditions on the changes in the microstructural features and mechanical performance of HSLA steel [8-10]. The inherent protection capabilities of Al and Nb are well-documented, but the impact of small alloying addition on the corrosion behaviour of steel requires further attention. Individual studies [14, 15] observing small increases in Al and Nb contents have shown to enhance steel protection through surface product formation, although the mechanisms influencing this behaviour, including microstructure, are not clear and require a better understanding. Additionally, the synergistic effect of multi-microalloying for both elements, which have contradictory effects on the microstructure, has not been investigated in the context of sulfuric acid corrosion resistance and thus, evaluated in this paper. All the proposed changes in alloying composition and thermal history are associated with major changes in the microstructural features. As of yet, the relationship between these features and corrosion behaviour is not a definitive one. Chen and Zhang [16] reported that refinement of grain size of HSLA steel improves corrosion resistance considerably. Hadzima et al. [17] claimed that changing grain size in hot rolled ferritic steel did not have any effect on corrosion resistance. However, Li et

al. [18] observed that finer grain size in low carbon steel reduced corrosion resistance and this was ascribed to the higher number of active sites in the grain boundaries during corrosion. This uncertainty in the literature on the effect of microstructural characteristics on corrosion behaviour led to the current work to enhance understanding of processing-microstructure-corrosion relationship. The microstructure and chemical composition of a material are not independent of one another yet, rarely are they studied in conjunction.

The present paper aims to investigate micro-alloying HSLA steel with Al, Nb and their combination as well as the effect of the most significant processing parameters, including rolling condition and cooling rate on the microstructural characteristics including grain size, phase volume fraction and grain boundary carbides, using optical and scanning electron microscopes. Moreover, the corrosion behaviour of the HSLA steel is examined in a 10 wt% sulfuric acid medium via electrochemical techniques and materials characterisation techniques. The study will evaluate the effect of the microstructural changes, induced by alloying and heat treatment optimisation, on the corrosion behaviour of HSLA steel.

2. Experimental

2.1 Materials and composition

Laboratory vacuum melts were produced as 60kg ingots by Tata Steel; the composition analysis and processing parameters of the five steels are given in **Table 1**. The base composition (wt%) was ~0.06% C, 0.5% Si, 1.4% Mn. Generally, only a small amount of Al is added to commercial steel, 0.02-0.04%, for its de-oxidant benefits, for H1 steel, and will be used for comparison purposes to confirm whether a high Al addition 0.16%Al, for H2 steel, is beneficial to corrosion behaviour. To identify optimisation potential in corrosion resistance, H2 steel was further enriched with an additional 0.018%Nb, for H3 steel, whilst it is common to find 0.015-0.03%Nb in commercial steels. The contents of Al and Nb were selected based on their previous reported benefits to mechanical properties; 0.16%Al is the optimum content needed to improve impact behaviour while its combination with 0.018%Nb promotes strength considerably [8-10]. This is to explore any further benefits to corrosion behaviour.

2.2 Processing conditions

The 0.018%Nb bearing steel was selected to investigate the effect of rolling condition and cooling rate (**Table 1**). After casting, the ingots were soaked at 1250°C in a furnace then rolled, finish rolling at 950°C for the hot rolling condition, for H3 steel, and 800°C for the controlled rolling condition, for C3 steel. In order to investigate the effect of cooling rate after rolling, the hot rolled plates were cooled at 33 and 17°C min⁻¹, for steels H3 and H4, respectively. The ingot was rolled by a powerful four-roll mill having two back up rolls and two smaller working rolls. The rolling schedules for the hot and controlled rolling are presented in **Figure 1(a,b)**, respectively. Heat treatments are based on commercial rolling practice. The current steel plates have been produced by Tata steel in the UK using the current heat treatment process to produce steel products that are available in the global market and used in various applications. After rolling, the plates were left to cool in the air rather than quenching to avoid the formation of lower transformation products, such as martensite, that normally form at fast cooling rates, for example, when using water or oil [9]. The cooling rate is based on the plate thickness, the most

common plate thicknesses in the market are 15 and 30mm, with cooling rates of 33 and 17°C min⁻¹, respectively.

Table 1. Composition (wt%), rolling condition and cooling rate of the HSLA steels chosen for examination.

| Steel | Rolling condition | Cooling rate (°C min ⁻¹) | C | Mn | Si | S | P | Nb | Al | N |
|-------|-------------------|--------------------------------------|-------|------|------|--------|-------|-------|------|-------|
| H1 | HR* | 33 | 0.051 | 1.4 | 0.46 | 0.0043 | 0.005 | - | 0.02 | 0.009 |
| H2 | HR | 33 | 0.06 | 1.4 | 0.47 | 0.0045 | 0.005 | - | 0.16 | 0.007 |
| H3 | HR | 33 | 0.056 | 1.39 | 0.46 | 0.0046 | 0.005 | 0.018 | 0.16 | 0.006 |
| H4 | HR | 17 | 0.062 | 1.38 | 0.49 | 0.0041 | 0.004 | 0.018 | 0.17 | 0.007 |
| C3 | CR ⁺ | 33 | 0.056 | 1.39 | 0.46 | 0.0046 | 0.005 | 0.018 | 0.16 | 0.006 |

HR*: hot rolling, CR⁺: controlled rolling.

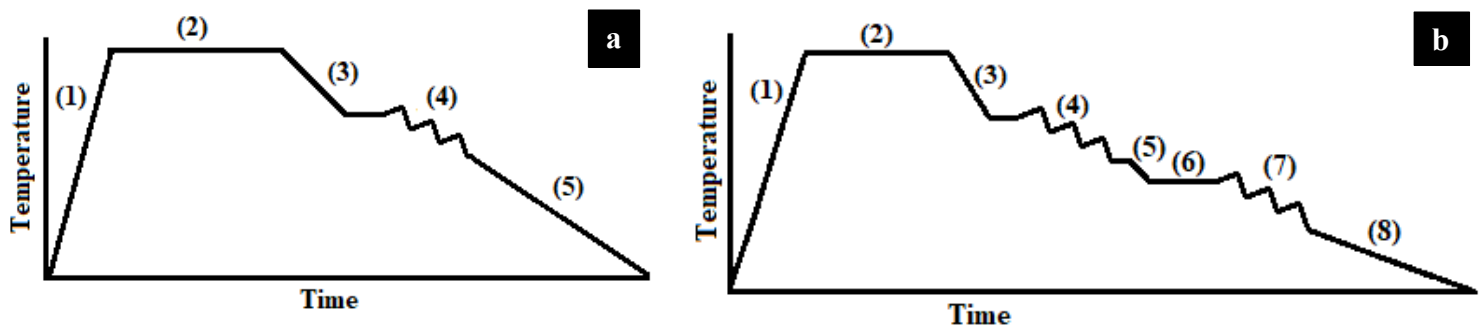


Figure 1. Schematic diagram of (a) the hot rolling process: 1) Heating from room temperature to soaking temperature 1250°C; 2) Held at soaking temperature; 3) Gap time to receiving the billet from the furnace to the mill; 4) Deformed at temperatures in the range 1100°C to 950°C; 5) The plates were then air cooled after rolling to the desired thickness, (b) the controlled rolling process: 1) Heating from room temperature to soaking temperature 1250°C; 2) Held at soaking temperature; 3) Gap time to receiving the billet from the furnace to the mill; 4) Deformed at temperatures in the range 1100°C to 1030°C; 5) Lowering the temperature to 950°C; 6) Held at this temperature; 7) Deformed at temperatures in the range 950°C to 800°C; 8) The plates were then air cooled after rolling to the desired thickness.

2.3 Sample preparation

The samples for analysis were grounded mechanically using SiC abrasive papers from 220 to 600 grit, followed by polishing the surface with 6 and 1µm diamond paste, respectively. The surface to be examined was rinsed with distilled water and subsequently cleaned with ethanol after each grinding and polishing step. Before the testing, the specimen was placed in an ultrasonic cleaner for 10 minutes. To observe the microstructural features, samples were etched with 2% Nital.

2.4 Surface analysis before corrosion

Optical microscope examinations were carried out using a Keyence VHX-7000 series Digital Microscope to analyse the microstructure of the steels. The phase volume fraction and average

grain size were measured using digital image analysis software (Image J) and is based on area percentage (contrast) and the line intercept method, respectively. The measurements were repeated at random areas at a magnification of 5X and the average value was taken for better accuracy. The grain boundary carbide density was measured by counting the number of grain boundary carbides in a 20 mm linear traverse, a measurement method used by a previous study [19]. Scanning electron microscope (SEM) examinations were performed before the corrosion experiment to make a detailed analysis of the microstructure and were also performed after the corrosion experiment to analyse the morphology of the corroded surface. Examinations were carried out using JEOL 7800F Field Emission Scanning Electron Microscope (SEM) with an Oxford Instruments Ultimex 100 mm² detector for elemental analysis, the spatial resolution of the microscope was <50nm at 20kV accelerating voltage. The SEM was used to measure the thickness of the grain boundary carbides and to confirm the presence of lower transformation products. The thickness of 100 carbides was measured for each sample and the average value was taken.

2.5 Electrochemical corrosion examination

The electrochemical corrosion experimental set-up was a three-electrode electrochemical cell involving a specimen, a platinum wire, and a saturated calomel electrode (SCE) serving as the working, counter, and reference electrodes, respectively. The epoxy-mounted specimen, with a total exposed surface area of 1cm², was soldered to copper wire to produce an electrical connection to the potentiostat during immersion. The electrochemical corrosion behaviour of the specimen was investigated in a sulphuric acid solution (H₂SO₄) with a volume of 1000ml and a concentration of 10 wt%. Electrochemical corrosion of the specimen was observed using potentiodynamic polarisation and electrochemical impedance spectroscopy (EIS), conducted using Ametek PARSTAT 4000 Multichannel Potentiostat in combination with VersaStudio software. Upon reaching a stable open circuit potential (OCP), the specimen was polarised at a scan range of -0.25V (vs. OCP) to 2V_{SCE} and at a scan rate of 0.167mV/s. The EIS measurement was undertaken using a measurement range of 100 kHz - 10 mHz and amplitude of 10mV, after obtaining a stable OCP. For reliable measurements, three tests were performed for each composition/processing condition and all the tests were performed at room temperature.

2.6 Weight loss corrosion examination

The weight loss technique was also used in the present work for corrosion resistance measurements at room temperature. Each sample was immersed and kept in 1000ml 10 wt% sulphuric acid solution, then taken out later and washed with distilled water and dried. The weight of the samples was measured and recorded before and after immersion to calculate the weight loss. Equation 1 [20] was used to evaluate the corrosion rate.

$$\text{Corrosion rate (cm/year)} = \frac{W \times 8.76 \times 10^3}{T \times D \times A} \quad (1)$$

where W is the mass loss in g, T is the period of immersion in hours, D is the density of the material (7.83g/cm³) and A is the area of the exposed surface in cm².

2.7 Analysis of the surface

XPS analysis was performed to further analyse the corroded surfaces of the hot rolled steels H1, H2 and H3 to determine the corrosion products formed on the surface using a Thermo

NEXSA XPS fitted with a monochromated Al $\kappa\alpha$ X-ray source (1486.7 eV), a spherical sector analyser and a 3 multichannel resistive plate, 128 channel delay line detectors. All data was recorded at 19.2W and an X-ray beam size of 400 x 200 μm . Survey scans were recorded at a pass energy of 200 eV, and high-resolution scans recorded at a pass energy of 40 eV. Electronic charge neutralisation was achieved using a Dual-beam low-energy electron/ion source (Thermo Scientific FG-03). Ion gun current = 150 μA . Ion gun voltage = 45 V. All sample data was recorded at a pressure below 10^{-8} Torr and a room temperature of 294 K. Data were averaged over 40 scans.

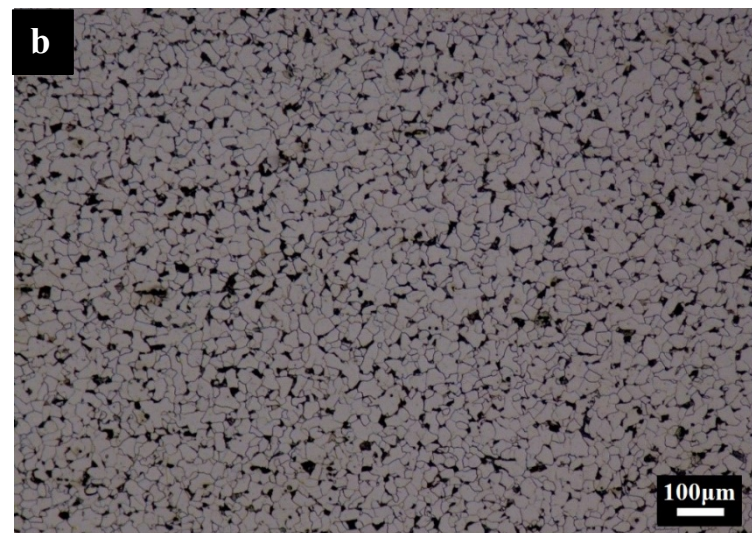
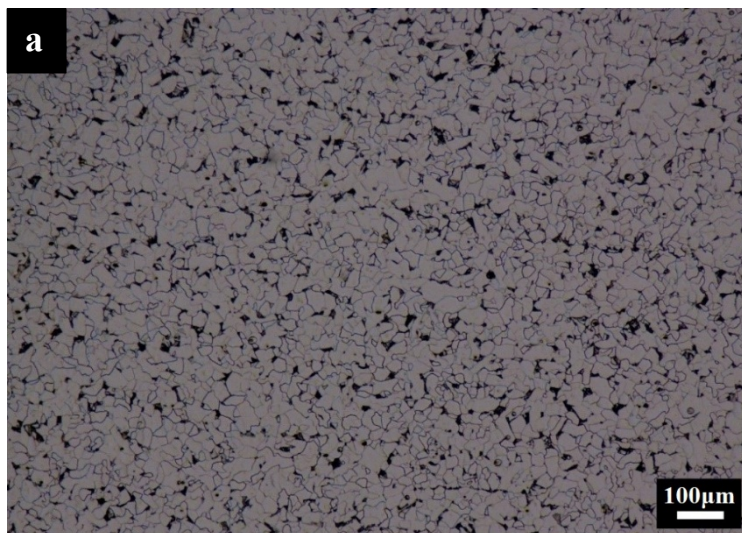
2. Results

3.1 Optical Microscopy

The microstructure of each of the steel samples was observed. The microstructures of the hot rolled steels at $33^\circ\text{C min}^{-1}$ for 0.02%Al, 0.16%Al and 0.16%Al-0.018%Nb are shown in **Figure 2(a-c)**, respectively, demonstrating a pearlite-ferrite microstructure. The microstructures were found to be relatively similar, with the increase of Al addition showing negligible influence on the average grain size, 24.4 and 23.7 μm for the 0.02%Al and 0.16%Al steels (**Figure 2(a,b)**), whilst increasing the pearlite phase fraction from ~ 5 to 8%, respectively (**Table 2**). However, the addition of Nb influenced the grain size distribution from a homogeneous to a heterogeneous distribution (a mixture of fine and coarse grains). The overall average grain size was significantly refined from 23.7 to 14.8 μm (**Figure 2(b,c)**) and the volume fraction of pearlite decreased from ~ 8 to 4%.

The microstructures of the hot rolled 0.16%Al-0.018%Nb steel at both cooling rates (33 and $17^\circ\text{C min}^{-1}$) are shown in **Figure 2(c,d)**, respectively. Reducing the cooling rate resulted in the growth of the average grain size from 14.8 to 18.3 μm .

The microstructures of the hot and controlled rolled steels at $33^\circ\text{C min}^{-1}$ for the 0.16%Al-0.018%Nb steel are shown in **Figure 2(c,e)**, respectively. The controlled rolling condition refined the average grain size further from 14.8 to 12.6 μm . In the hot rolling condition, all the grains have an equiaxed shape (**Figure 2c**) but a mixture of equiaxed and elongated grains is found in the controlled rolling condition, a row of elongated grains toward the rolling direction is arrowed (**Figure 2e**).



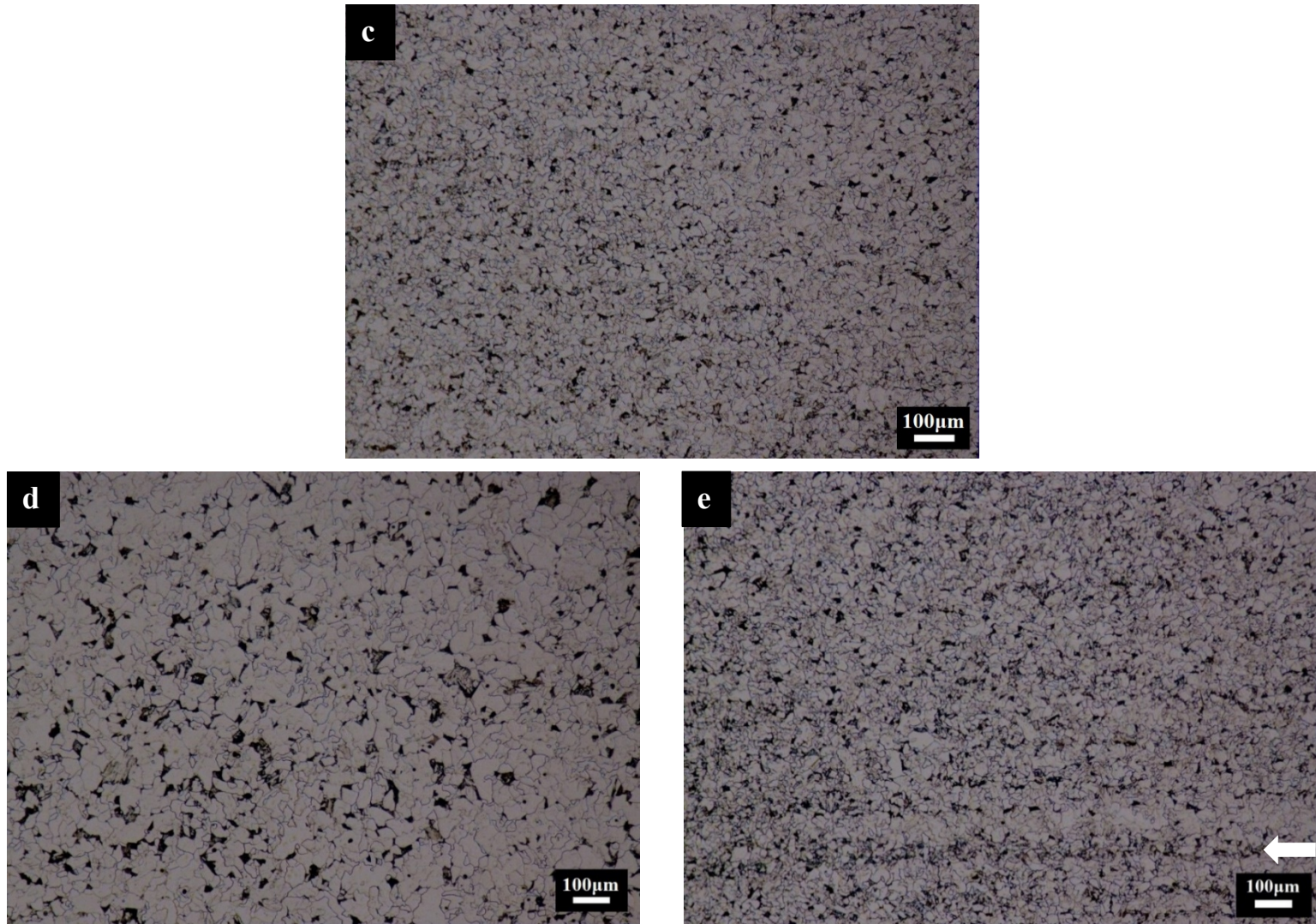


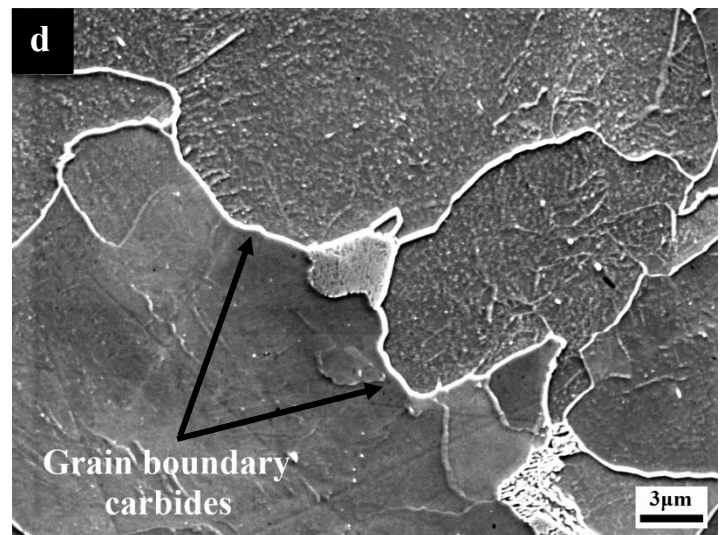
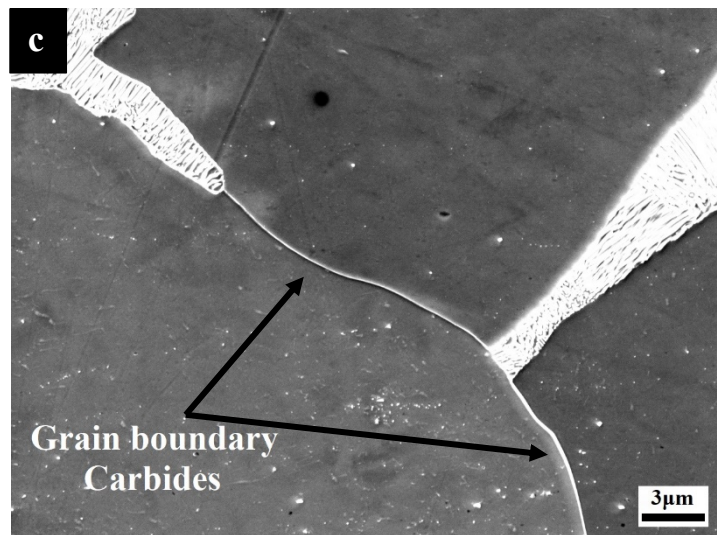
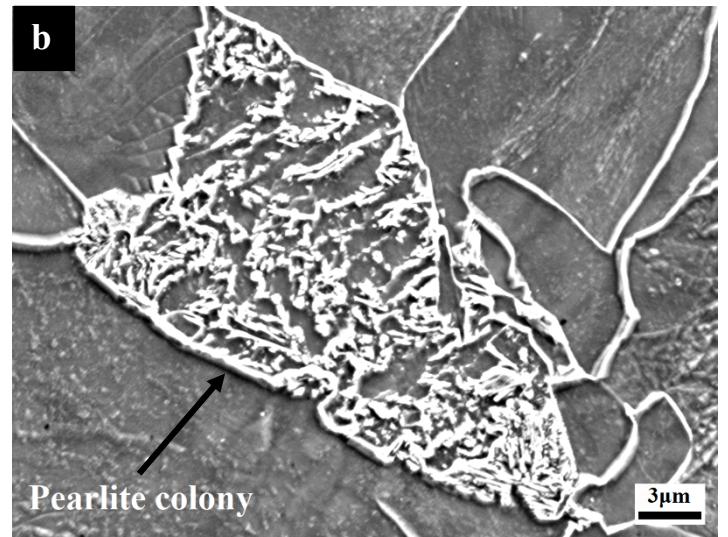
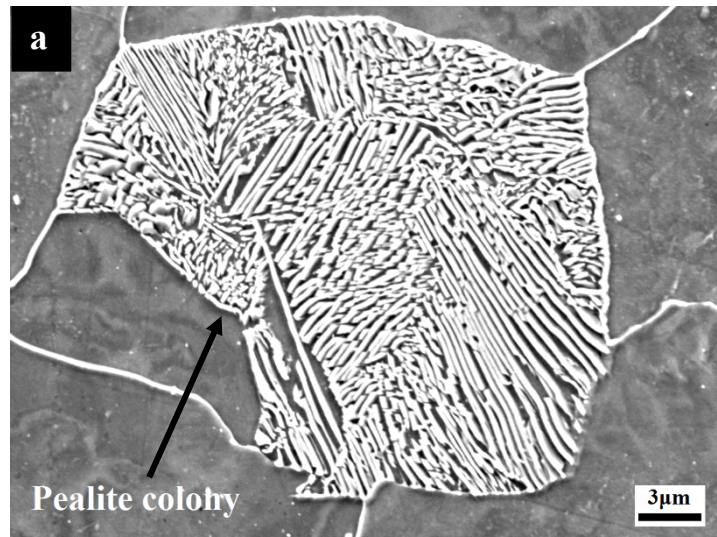
Figure 2. Optical microstructures of (a) 0.02%Al, (b) 0.16%Al, (c) 0.16%Al-0.018%Nb, (all under hot rolling condition at $33^{\circ}\text{C min}^{-1}$), and (d) 0.16%Al-0.018%Nb at $17^{\circ}\text{C min}^{-1}$, and (e) 0.16%Al-0.018%Nb under controlled rolling, a row of elongated grains is arrowed.

3.2 SEM examination of the microstructure before corrosion

Typical pearlite colonies of the 0.16%Al and 0.016%Al-0.018%Nb bearing steels are shown in **Figure 3(a,b)**. The plate carbides in the pearlite colony of the 0.16%Al steel exhibit a much straighter, and regular crystallographic orientation (**Figure 3a**), whilst the plate carbides in the 0.016%Al-0.018%Nb bearing steel do not have a uniform shape and they do not follow a specific pattern (**Figure 3b**). Furthermore, the pearlite colonies in the 0.16%Al bearing steel are found to be saturated with cementite but the addition of Nb reduced the volume fraction of cementite considerably (**Figure 3(a,b)**).

Typical grain boundary carbides of the 0.16%Al and 0.016%Al-0.018%Nb bearing steels are shown in **Figure 3(c,d)**. It is observed that adding 0.018%Nb significantly altered the density and more importantly the thickness of the grain boundary carbides. The Nb addition coarsened the carbides from 0.21 to $0.3\mu\text{m}$ and increased their density from 14.1 to 18.9N mm^{-1} (**Table**

2). AlN precipitates were present in the hot rolled 0.16%Al bearing steel, a typical AlN precipitate is presented in **Figure 3(e,f)**. The microstructure of the hot rolled 0.16%Al-0.018%Nb bearing steel confirming the presence of martensite is shown in **Figure 3g**.



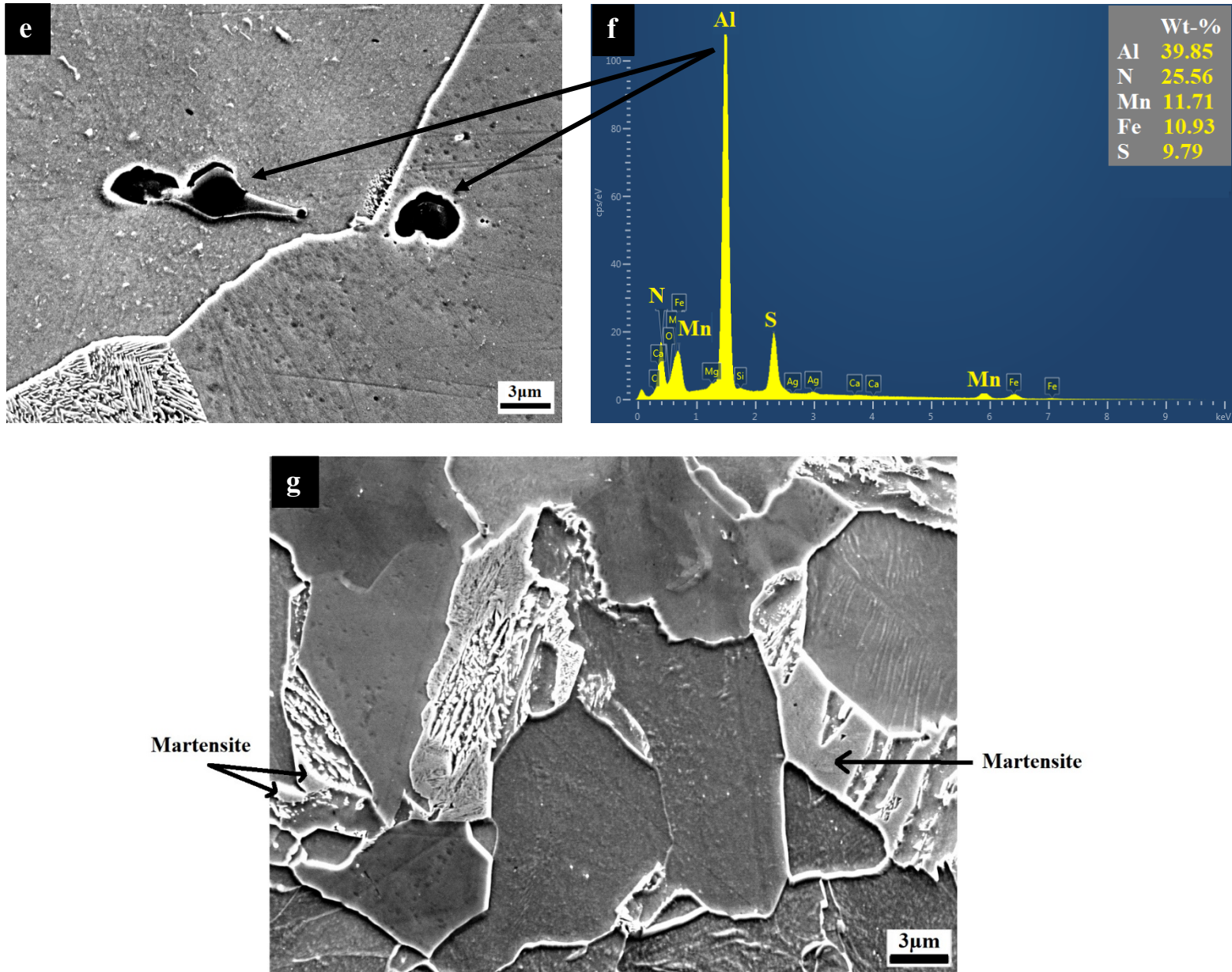


Figure 3. SEM micrographs showing, typical pearlite colony of the hot rolled steels for (a) 0.16%Al, (b) 0.16%Al-0.018%Nb, typical grain boundary carbides of the hot rolled steels for (c) 0.16%Al, (d) 0.16%Al-0.018%Nb, the hot rolled 0.16%Al bearing steel with (e) typical AlN precipitates, (f) EDS analysis spectrum, and (g) the presence of martensite in the hot rolled 0.16%Al-0.018%Nb bearing steel.

Based on the analysis of the optical and SEM micrographs the following data; average grain size, volume fraction of phases, thickness and density of grain boundary carbides are summarised in **Table 2** for subsequent discussion.

Table 2 Summary of the analysis of the optical and SEM micrographs.

| Steel | Rolling condition | Cooling rate (°C min ⁻¹) | Nb (wt%) | Al (wt%) | N (wt%) | Grain size (μm) | Pearlite (%) | Carbide thickness (μm) | Carbide density (N mm ⁻¹) | Martensite |
|-------|-------------------|---|-------------|-------------|------------|--------------------|-----------------|---------------------------|--|------------|
|-------|-------------------|---|-------------|-------------|------------|--------------------|-----------------|---------------------------|--|------------|

| | | | | | | | | | | |
|-----------|-----------------|----|-------|------|-------|------|-----|------|------|---|
| H1 | HR* | 33 | - | 0.02 | 0.009 | 24.4 | 4.8 | 0.25 | 16.2 | - |
| H2 | HR | 33 | - | 0.16 | 0.007 | 23.7 | 7.9 | 0.21 | 14.1 | - |
| H3 | HR | 33 | 0.018 | 0.16 | 0.006 | 14.8 | 4.1 | 0.30 | 18.9 | ✓ |
| H4 | HR | 17 | 0.018 | 0.17 | 0.007 | 18.3 | 4.0 | 0.32 | 17.1 | ✓ |
| C3 | CR ⁺ | 33 | 0.018 | 0.16 | 0.006 | 12.6 | 5.0 | 0.23 | 21.8 | - |

HR*: hot rolling, CR⁺: controlled rolling.

3.3 SEM examination of the corroded surface

The SEM micrographs of the corroded surfaces of the hot rolled steels 0.02%Al, 0.16%Al and 0.16%Al-0.018%Nb are shown in **Figure 4**. The 0.02%Al bearing steel experienced a relatively higher level of pitting, as indicated by the high volume fraction of deep pits spread throughout the surface (**Figure 4a**). Increasing the Al content to 0.16%Al minimised the pitting attack considerably by reducing the amount and depth of the pits (**Figure 4b**). A combination of 0.16%Al and 0.018%Nb contributed further in restricting the pitting attack, as observed by the reduction of the volume fraction and depth of the pits (**Figure 4c**).

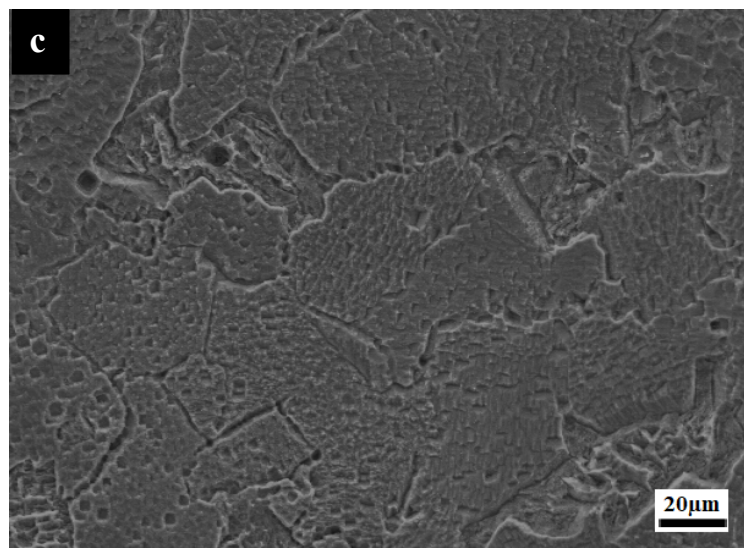
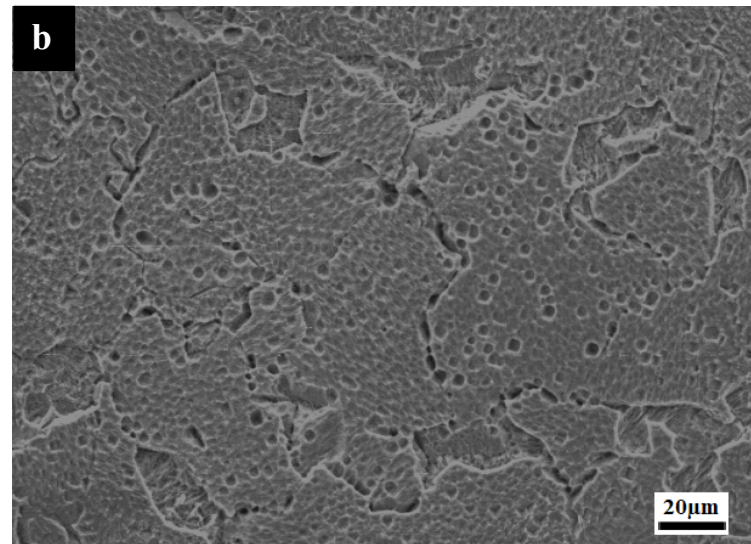
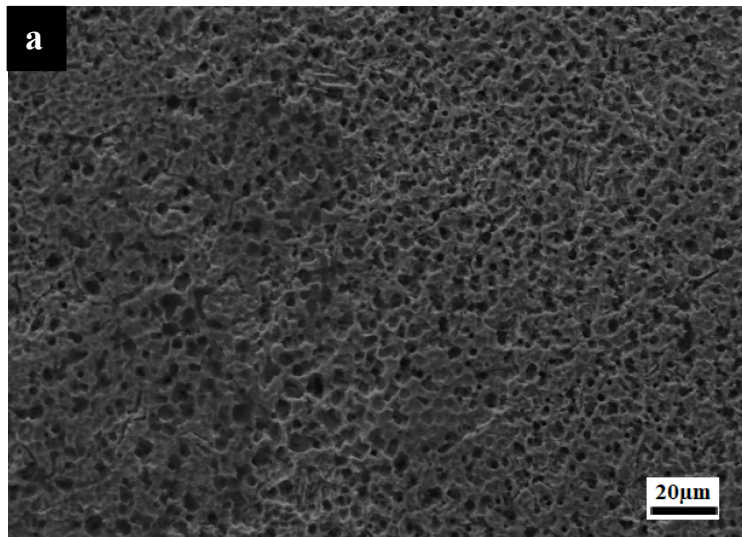


Figure 4. SEM micrographs showing the corroded surfaces of the hot rolled steels for **(a)** 0.02%Al, **(b)** 0.16%Al, **(c)** 0.16%Al-0.018%Nb.

3.4 Corrosion results

Composition

Figure 5a displays the potentiodynamic polarisation curves of the three hot rolled steels, which allows for analyses of the differences in corrosion behaviour. All the three steels show almost negligible differences in corrosion behaviour during the activation stage. The 0.02%Al bearing steel shows severe pitting corrosion, indicated by the noise shown throughout the passivation region. It can be observed, however, that the addition of 0.016%Al minimised pitting attack as indicated by the noise reduction at the same potential range as well as decreasing the current density during the passivation stage, and is even further improved with the addition of Nb. This behaviour indicates an improvement in corrosion behaviour with increasing the alloying content through passive film formation (lower anodic dissolution) within this region showing higher stability, likely due to surface enrichment. Thereafter, the active dissolution behaviour demonstrated in the potentiodynamic curve indicates the breakdown of the passive film, which occurs at very similar potential values for all three steels, $\sim 1.6\text{V}$.

Al and Nb are shown to be effective in promoting the charge transfer resistance in both regions; transition region and passivation region. The transfer from the active to the transition region occurred earlier at a lower potential and the passivation range was widened due to the early start of the passivation at a lower potential by increasing the Al content while a combination of both Nb and Al reduced the transition potential and expanded the passivation range further (**Figure 5a**).

Figure 5b shows the Nyquist plots for the impedance spectra undertaken at open circuit potential for the three hot rolled steels. The length of the arc diameter is consistently increased with an increase in the Al content and the addition of Nb, suggesting an improvement in corrosion resistance; this is in line with the polarisation behaviour in **Figure 5a** and weight loss measurements (**Figure 8**).

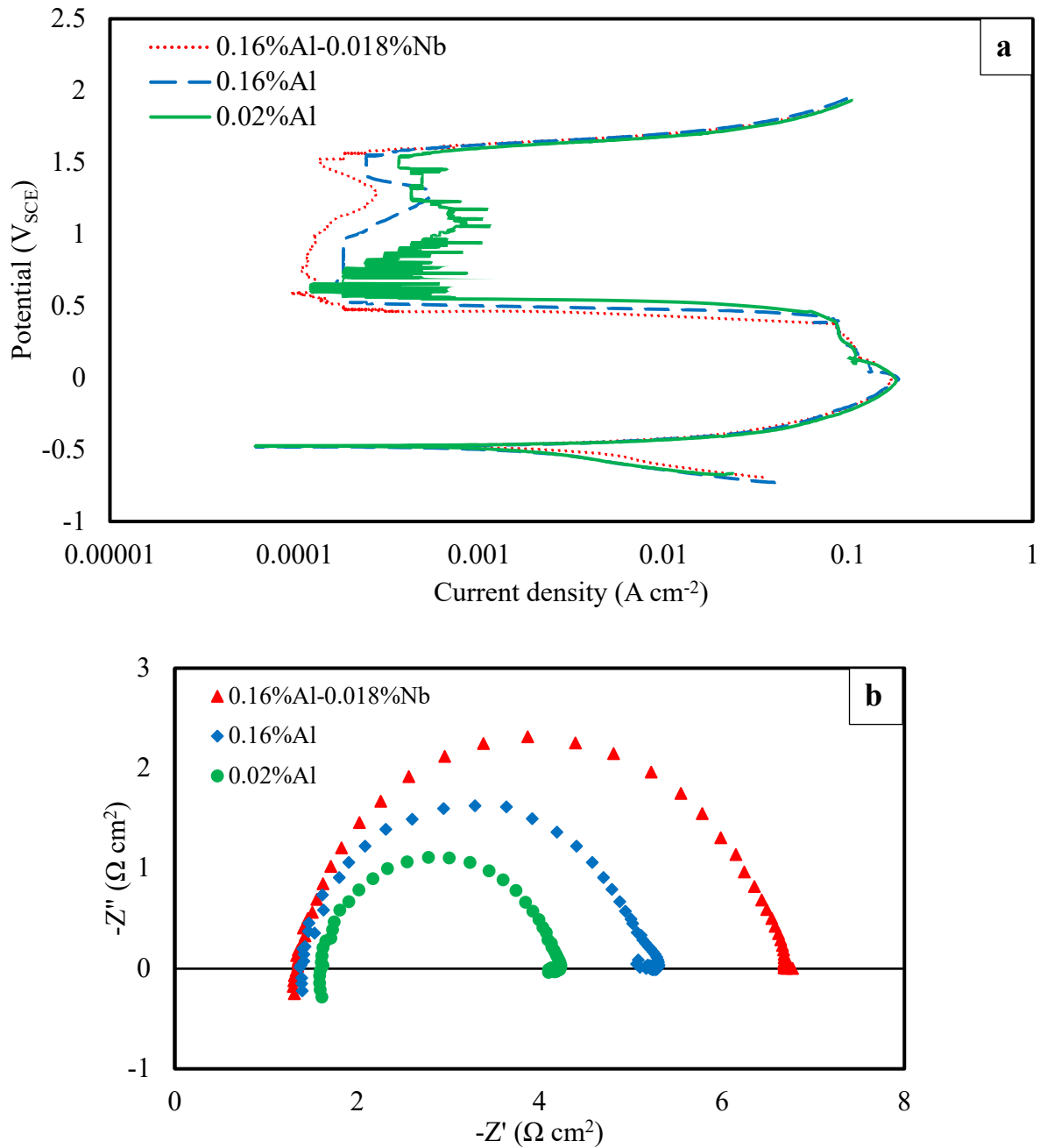


Figure 5. Electrochemical corrosion data for the hot rolled steel at 33°C min⁻¹ for 0.02%Al, 0.16%Al and 0.16%Al-0.018%Nb: **(a)** Potentiodynamic polarisation curves, **(b)** Nyquist plots.

Cooling rate

The potentiodynamic polarisation curves and Nyquist plots of the 0.16%Al-0.018%Nb bearing steel at both cooling rates (17 and 33°C min⁻¹) are presented in **Figure 6(a,b)**, respectively. Reducing the cooling rate is shown to be effective to shift the passivation region to a lower current density (**Figure 6a**). At slow cooling, the diameter of the semicircle is larger, indicating that reducing the cooling rate improves corrosion resistance (**Figure 6b**).

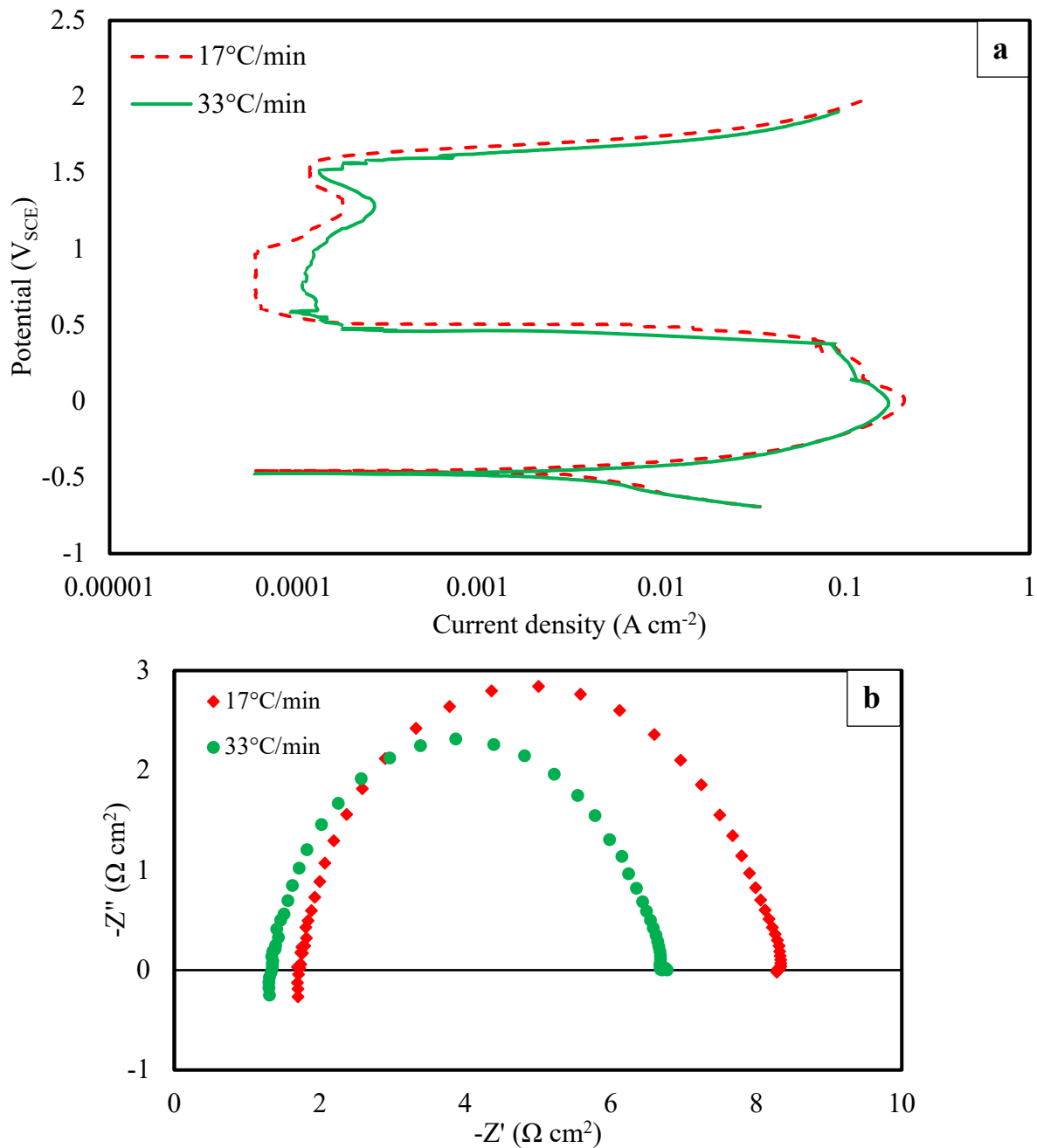


Figure 6. Electrochemical corrosion data for the hot rolled steel 0.16%Al-0.018%Nb steel at both cooling rates (17 and $33^{\circ}C\ min^{-1}$): **(a)** Potentiodynamic polarisation curves, **(b)** Nyquist plots.

Rolling condition

The potentiodynamic polarisation curves and Nyquist plots of the 0.16%Al-0.018%Nb bearing steel at both rolling conditions (hot and controlled rolling) are shown in **Figure 7(a,b)**, respectively. The corrosion behaviour is similar throughout the active and transition regions (**Figure 7a**). However, the controlled rolled steel passivated to a lower current density in the passivation region in comparison with the hot rolled steel. The Nyquist plots also show that controlled rolling gave a higher resistance to charge transfer, indicated by the larger diameter of the controlled rolled steel (**Figure 7b**).

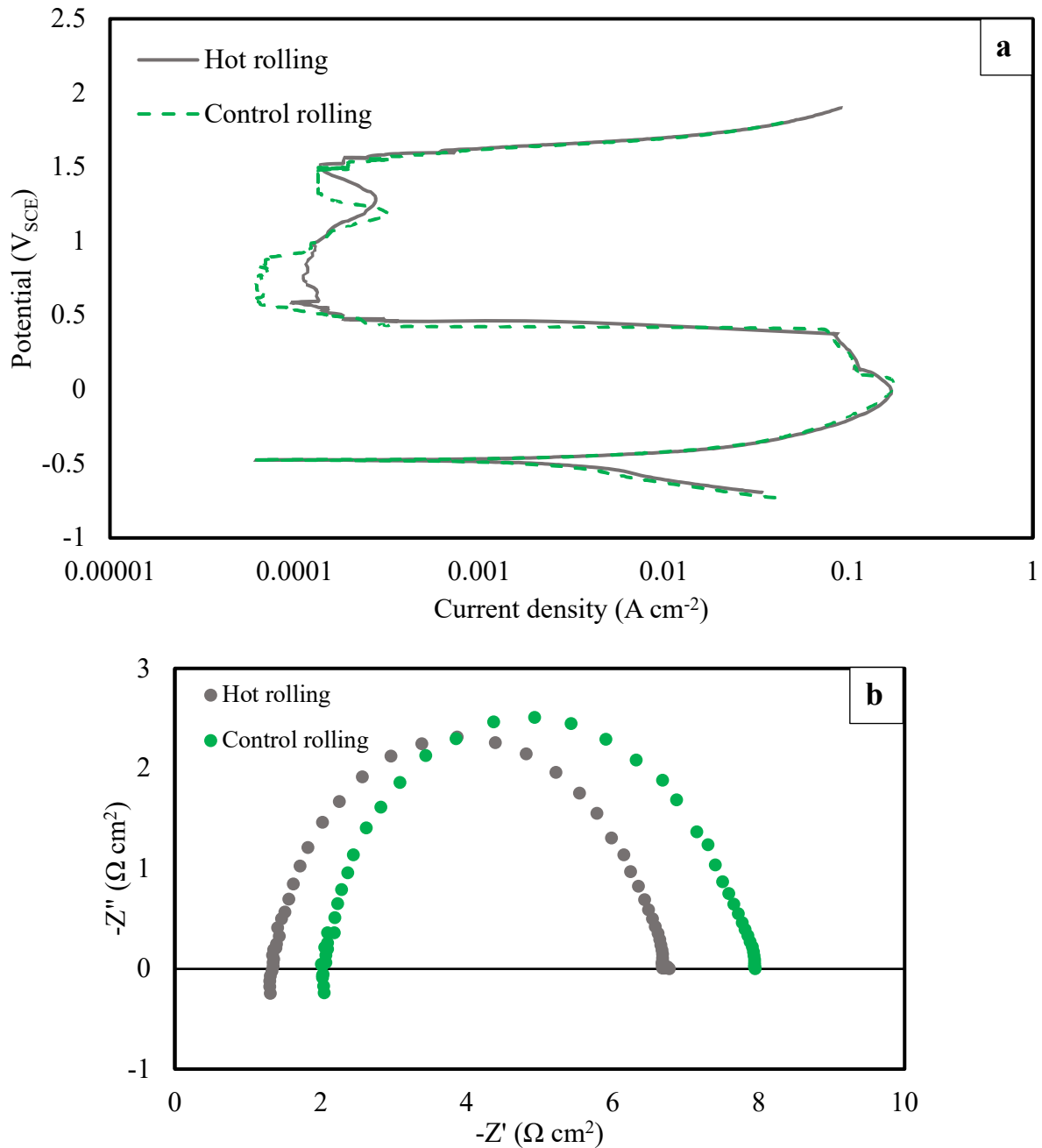


Figure 7. Electrochemical corrosion data for the hot rolled 0.16%Al-0.018%Nb steel at both rolling conditions (hot and controlled rolling): **(a)** Potentiodynamic polarisation curves, **(b)** Nyquist plots.

Corrosion current density i_{Corr} and corrosion potential E_{Corr} were obtained from the extrapolation of the anodic and cathodic Tafel lines in the potentiodynamic polarization curves, and presented in Table 3.

Table 3 Corrosion current density (i_{Corr}) and corrosion potential (E_{Corr}) obtained from the potentiodynamic polarization curves for the examined HSLA steels.

| Steel | Rolling condition | Cooling rate ($^{\circ}\text{C min}^{-1}$) | Nb (wt%) | Al (wt%) | N (wt%) | E_{Corr} (mV _{SCE}) | i_{Corr} (mA cm ⁻²) |
|-------|-------------------|---|-------------|-------------|------------|---|---|
|-------|-------------------|---|-------------|-------------|------------|---|---|

| | | | | | | | |
|-----------|-----------------|----|-------|------|-------|------|-------|
| H1 | HR* | 33 | - | 0.02 | 0.009 | -475 | 3.171 |
| H2 | HR | 33 | - | 0.16 | 0.007 | -478 | 2.881 |
| H3 | HR | 33 | 0.018 | 0.16 | 0.006 | -469 | 2.755 |
| H4 | HR | 17 | 0.018 | 0.17 | 0.007 | -462 | 2.530 |
| C3 | CR ⁺ | 33 | 0.018 | 0.16 | 0.006 | -463 | 2.604 |

Weight loss

The measurements taken by the weight loss technique are in agreement with the electrochemical measurements. Increasing the Al content reduced the corrosion rate, and a combination of both Al and Nb improved the corrosion resistance further (**Figure 8**). Moreover, lowering the cooling rate of the 0.16%Al-0.018%Nb steel, reduced the corrosion rate, in the case of rolling, controlled rolling was found to give lower corrosion rate than hot rolling as presented in **Figure 8**. Generally, the influence of optimising the composition on corrosion behaviour is more pronounced than optimising the processing conditions. In summary, a combination of both 0.16%Al and 0.018%Nb resulted in the lowest corrosion rate and this is enhanced further by reducing the cooling rate and processing the steel under controlled rolling condition.

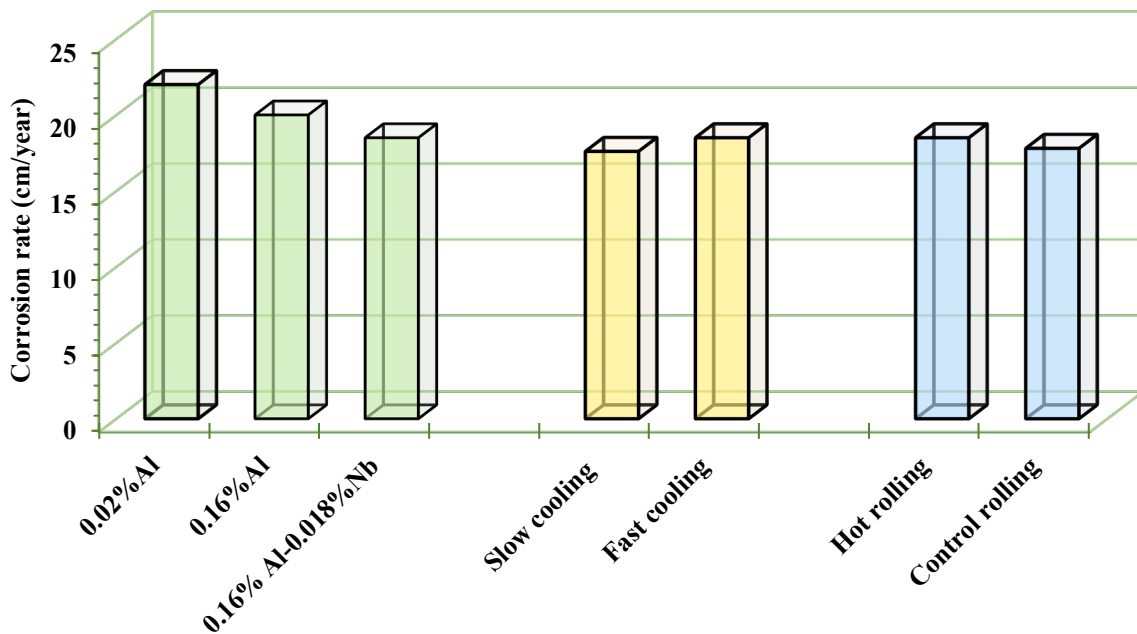


Figure 8. The corrosion rates based on the weight loss method of the examined steels 0.02%Al, 0.16%Al and 0.016-0.018%Nb, and 0.16-0.018%Nb at both cooling rates; 17 and 33°C min⁻¹, and 0.16-0.018%Nb at both rolling conditions (hot and controlled rolling).

2.5 Surface analysis

XPS was employed to evaluate the composition of the products formed on the surface of the hot rolled steels at different alloying compositions at the corrosion potential, in the passivation range. A summary of the composition data of the surface products is presented in **Table 4**. In

general, the analysis indicates the presence of Fe, C, O, S and Si on the surface of all the steels independent of the composition, and for H3-steel Nb was detected. The addition of Al is shown to encourage the precipitation of carbide, iron and oxide into the surface by increasing their contents in the layer composition, for H2-steel. A combination of both Al and Nb promoted carbide, iron and oxide precipitation, and an additional benefit is observed by the presence of Nb on the surface of the H3-steel.

Table 4. Summarised XPS data for surface products of the examined hot rolled steels at 33°C min⁻¹, (%).

| Steel | Composition | Fe | C | O | S | Si | Nb |
|-------|------------------|-----|------|------|------|------|-----|
| H1 | 0.02%Al | 6.9 | 33.8 | 36 | 13.2 | 10.1 | 0 |
| H2 | 0.16%Al | 9.6 | 35.8 | 37.7 | 9.5 | 7.4 | 0 |
| H3 | 0.16%Al-0.018%Nb | 9.8 | 38.1 | 39.6 | 7.3 | 4.4 | 0.8 |

3. Discussion

4.1 Composition

The effect of increasing Al content

Increasing the Al content was found to improve the corrosion resistance considerably by extending the passivation potential range and passivating at a lower current density (**Figure 5a**). The increase of the arc diameter of the Nyquist plot at the high Al content indicates the suppression of charge-transfer, leading to higher corrosion resistance (**Figure 5b**), which is also confirmed by the decrease of the current density (**Table 3**).

When discussing the influence of Al, N has also to be taken account of because Al is a strong nitride forming element. In the case of the 0.02%Al bearing steel, N remains in solution rather than precipitating out since no AlN precipitates were observed under the SEM examination. However, increasing the Al content to 0.16% encouraged precipitation of AlN as shown in **Figure 3(e,f)**, as the driving force for precipitation becomes higher and thus Al can remove N from solution [8].

Previous work [21] reported that the corrosion behaviour of steel is affected considerably by the presence of nitrogen in the composition. The work showed that nitrogen improves the corrosion behaviour of steel when it is present in a solid solution. Therefore, it is expected that the removal of N by Al in the current work would reduce the corrosion resistance. However, the role of Al on the microstructure is not limited to AlN precipitation but involves other factors that should be considered when evaluating its influence on corrosion behaviour.

Since the high Al bearing steel obtained a high volume fraction of pearlite, ~8% at 0.16%Al and ~5% at 0.02%Al (**Table 2**), it would also be expected that the high Al bearing steel would give lower corrosion resistance due to the higher fraction of galvanic cells induced between ferrite and cementite in pearlite [22]. However, the microstructural measurements show that higher pearlite volume fraction is associated with less and thinner carbides at the grain boundaries (**Figure 2(a,b)** and **Figure 3(c,d)** and **Table 2**). This is because pearlite acts as a feedstock for grain boundary carbides, this is indicated by the SEM micrographs (**Figure 3a,b**), which show that grain boundary carbides are not isolated but often attached to the pearlite colonies. This means that although the high Al bearing steel obtained the highest volume

fraction of pearlite, this is associated with the lowest and finest grain boundary carbides. Al contributes to slowing down the diffusion rate of carbon at the grain boundaries. In earlier work, Al was reported to lower the pearlite start transformation temperature so giving less time for carbides to develop at the boundaries [19]. In the corrosive media, the attack concentrates on the grain boundary carbides leading to intergranular corrosion and hence higher corrosion rate. However, the refinement of grain boundary carbides by Al contributes markedly in promoting corrosion resistance. In addition, Al is an effective element in enhancing the formation of a stable passive layer, which is rich in carbide and oxide (**Table. 4**), that is shown to enhance passivation behaviour (**Figure 5a**) and minimise pitting corrosion (**Figure 4b**).

Previous work [23] reported a marked improvement in toughness with the addition of 0.16%Al. Therefore, the addition of Al is beneficial in enhancing both mechanical properties and corrosion behaviour, simultaneously. However, Al content should always be restricted because higher additions, >0.16%Al, would favour the formation of martensite, which in turn deteriorates the corrosion resistance, as well as toughness [24]. Therefore, the addition of 0.16%Al is recommended to achieve the optimum balance in mechanical properties and corrosion behaviour.

The effect of the addition of Nb

The high Al content and Nb addition are effective in obstructing pitting attack that is experienced by the low Al bearing steel. Initially, the pits initiate on the surface at the beginning of the corrosive attack, they begin to expand and develop, and their volume increases over time. However, as Nb is added and Al content increases, the severity of the attack decreases so it becomes more difficult for the pits to develop further and fewer pits are able to initiate as indicated by the SEM morphologies (compare **Figure 4a** with **Figure 4(b,c)**). Moreover, the considerable noise present throughout the passive potential range in the polarization curve of the low Al bearing steel confirms the severity of the pitting attack, which is minimised upon adding Nb and increasing Al content (**Figure 5a**). The severe pitting attack can be attributed to the weak protective layer that forms in the low Al containing steel, indicated by its passivation at a high current density, (**Figure 5a**), in comparison with the high Al and Nb containing steels that form reliable and adherent passive films that obstruct the electrolyte penetration and so giving less current density (**Figure 5(b,c)**). Since the separate addition of Al and Nb enhances the corrosion resistance by the formation of a protective layer on the surface, it is expected that the current steel containing both Al and Nb would have a stronger protective layer that minimises the corrosion attack concentration on the grain boundary carbides.

Careful control of alloying composition and heat treatment was taken in order to keep the microstructure consistent in all the steels. Previous work [8] reported that higher contents of Nb and Al encourage the formation of lower transformation products in the microstructure; martensite and bainite. Increasing the cooling rate after rolling the plate by using water or oil quenching, or having thin steel plates also encourage lower transformation products to form. In the current work, the contents of C, Al and Nb were kept low, 0.06, 0.16 and 0.018%, respectively, and the steel plates were air cooled to reduce the cooling rate. This is important to ensure the prevention of lower transformation products, in order to standardise the phases for more reliable analyses. However, the current HSLA steel containing Nb still showed the formation of martensite in the microstructure as presented in **Figure 3g**. Although martensite was reported in previous work to reduce the corrosion resistance [25, 26], the current Nb containing steel gave the best corrosion behaviour among all the examined steels. However, it

must be appreciated that the low Nb and C contents and low cooling rate in the present work restricted the volume fraction of martensite to less than 1% in comparison with the previous work where the volume fraction of martensite was greater than 25% [26].

Nb is a strong carbide forming element, so it encourages the formation of NbCN precipitates [27]. NbCN is very effective in retarding grain boundary movement through pinning during rolling [28]. During cooling, the new ferrite phase nucleates on the austenite grain boundaries. Due to the considerable grain size refinement of the Nb bearing steel, nucleation of the ferrite phase is facilitated due to the availability of a higher fraction of boundaries [29]. Therefore, more nucleation sites prior to transformation become available and so the Ar₃ transformation occurs more readily at a higher temperature during solidification.

Generally, transformation temperature has a considerable effect on carbide development, in which higher transformation temperature would give more time for carbides to grow and thicken [30]. Grain boundary carbides are expected to give further deterioration in corrosion behaviour by setting up galvanic cells between the grain boundary carbides and ferrite grains, so accelerating the corrosion reaction, in which cementite acts as the cathode and ferrite as the anode. The changes in the microstructure due to Nb addition are expected to lower the corrosion resistance. Nb containing steel is found to have the finest grain size as well as the highest carbide thickness and density among all the examined steels (**Table 2**). All these microstructural features have a negative effect on corrosion behaviour. However, the addition of Nb coarsened the carbide thickness from 0.21 to 0.30 μm and increased their density from 14.1 to 18.9N mm⁻¹ (**Table 2**), which is not a significant difference, due to the insufficient C available to precipitate to the boundaries, 0.06%C.

The refinement of grain size is known to increase the corrosion rate due to the increased number of active sites in the grain boundaries [31]. However, Nb contributed to activate passivation, providing a protective film on the surface, that is rich in carbide, oxide and Nb, to enhance corrosion resistance (**Table 4**). This positive effect of the passive film overcame the negative effect of the refinement of grain size and also the coarsening of grain boundary carbides. Moreover, in the current work, both C and N were kept low enough, 0.06%C and 0.007%N, to restrict carbide development and grain size refinement, respectively.

The thickness and density of grain boundary carbides can be suppressed by increasing the cooling rate, for example, water quenching, so giving less time for carbide to precipitate out from the carbon-rich austenite to the boundaries and giving less time for carbides to grow during solidification [24]. However, this route is associated with two consequences; further refinement of grain size and formation of martensite, where both promote corrosion rate. It is worth mentioning that intergranular corrosion is still observed in the high Al and Nb containing steels (**Figures 4(b,c)**) which can be attributed to the presence of carbides at the grain boundaries, in which they become the preferred sites for corrosion concentration. Intergranular corrosion is a concern especially for alloys with high contents of C and N, so the C and N contents should be restricted especially in the presence of elements that have a high affinity for carbon and nitrogen such as Nb and Al.

4.2 Cooling rate

The nature of the microstructure and grain size evolution have been found to be influenced by the processing conditions [32, 33]. Lowering the cooling rate was found to improve corrosion resistance (**Figure 6**), and this was associated with the coarsening of grain size (**Figure 2(c,d)** and **Table 2**). Microstructural features such as phases present and their volume fraction did not vary except for the grain size and grain boundary carbides, which were refined by increasing the cooling rate (**Table 2**). Therefore, any changes to corrosion behaviour for the same composition can be attributed to variation in grain size and grain boundary carbides. Finer grain size is beneficial when considering mechanical properties; strength and ductility. This is due to the fact that grain boundaries impede further dislocation propagation during deformation. However, grain boundaries act in a different way under corrosive environments, where a higher density of boundaries enhances the corrosion rate. This can be a serious issue for the ultrafine-grained steels which have an average grain size between 1 and 2 μm , and are currently being developed to replace some conventional steels [34].

Li et al. [35] reported that the refinement of grain size in low carbon steel increased the corrosion rate and this was ascribed to the increased number of active sites in the grain boundaries during corrosion. Moreover, the finer grain size was reported to accelerate the dissolution rate of the steel in the corrosive electrolyte. The energy at the grain boundary is higher than the matrix and so encouraging the anodic reaction to take place preferably at the boundary [35].

Although fast cooling rates have the disadvantage of increasing the grain boundary density, it was found to reduce grain boundary carbide thickness (**Table 2**). Fast cooling rates are effective in lowering the A_{r3} temperature and as a result, less time becomes available for carbides to grow during transformation [36]. The finer grain size obtained at the fast cooling rate, by giving less opportunity for carbides to accumulate at the boundary through providing a higher fraction of boundary, also contributed to the carbide refinement.

These carbides are cathodic to ferrite, so expected to promote galvanic corrosion at the slower cooling rate [37]. However, the detrimental effect of the finer grain size on corrosion behaviour overcame the beneficial effect of the finer grain boundary carbides at fast cooling, the former being the dominant factor. Furthermore, it is worth mentioning that despite the finer grain boundary carbides observed at fast cooling, the density of these carbides was found to be higher than the slow cooling condition (**Table 2**), so the benefit of carbide refinement was lost due to their higher density. The denser grain boundary carbides at fast cooling give a higher tendency for intergranular corrosion to take place.

4.3 Rolling condition

Since rolled HSLA steels are processed through hot rolling and controlled rolling, the influence of the rolling condition on corrosion behaviour is of importance. The controlled rolling gave higher corrosion resistance than the hot rolling process (**Figure 7**). In order to investigate the causes, it is important to analyse the changes in the microstructural features at each rolling condition.

In controlled rolling, the steel plate is rolled below the non-recrystallisation temperature, which creates a high amount of dislocations. During transformation, ferrite nucleates preferably at these dislocations, so a finer ferrite grain size is achieved [9]. Upon refinement of grain size,

carbide thickness was shown to be thinner and denser due to the higher area fraction of grain boundary available for carbides to precipitate on.

Although the refinement of grain size and the denser grain boundary carbides were expected to reduce the corrosion resistance in the controlled rolled steel, as the case in fast cooling, the controlled rolled steel showed higher corrosion resistance in comparison with the hot rolled steel. It worth mentioning that changes in microstructural features upon changing the cooling rate from 17 and 33°C min⁻¹ are limited to grain size and grain boundary carbide development. The case of rolling condition is more complex, and other changes need to be considered.

At a constant composition, controlled rolling is effective in suppressing the formation of lower transformation products, mainly martensite while hot rolling process has a higher tendency to form such products, the SEM examination confirmed that martensite was present in the hot rolled steel, **Figure 3g**, which was absent in the controlled rolling condition. This is due to the difference in the Ar₃ temperature during cooling, at which controlled rolling raises the Ar₃ temperature due to the refinement of grain size so giving less opportunity for martensite to form [8]. In previous work, martensite was reported to give poor corrosion resistance in dual-phase steels [26]. This was also verified by Nadlene et al. [38] who observed a linear increase in corrosion rate as martensite volume fraction increases, through intercritical annealing process, in dual phase steel. The residual stresses that are induced by martensite are responsible for deteriorating the corrosion resistance [39], as well as the increase of the current flow due to the larger interfacial area between ferrite (anode) and martensite (cathode) [38].

The hot rolling process is conducted above the recrystallisation temperature. After each rolling pass, the deformed grains recrystallise so new grains nucleate at the boundaries of the deformed elongated grains, so providing equiaxed grain structure (**Figure 2c**). However, controlled rolling involves rolling the steel above and below the recrystallisation temperature and so giving a mixed microstructure of equiaxed and elongated directional grains (**Figure 2e**). The elongated directional grains have low-angle boundary in comparison with the equiaxed grains. Generally, controlled rolling provides a higher percentage of low-angle boundary than the hot rolling process and this is also confirmed by the SEM micrograph in **Figure 2e**. Previous work [40] performed deep analysis on misorientation between grains and corrosion behaviour and concluded that as the percentage of high-angle boundary increases the steel becomes more susceptible to corrosion. Although the previous work used Cr to control the orientation of the grains (1 - 4%Cr), where higher Cr contents gave lower angle boundary so improving corrosion resistance, this approach is not applicable to the current HSLA steel where the contents of the alloying elements are restricted to 2%. However, controlled rolling is found to be beneficial to compensate for the absence of Cr by optimising the misorientation distribution. Industrially, controlled rolled steels are preferred over the hot rolled ones when considering mechanical properties, where both strength and toughness are enhanced.

Therefore, it can be concluded that controlled rolling is one of the few processing conditions that can promote both mechanical properties and corrosion behaviour, so expanding the use of the steel in wider applications, where the steel can experience stress corrosion cracking.

4.4 Surface analysis

The current work included investigating the corrosion resistance based on the microstructure as well as passivation behaviour. The improvement of the passivation behaviour upon

increasing Al content from 0.02 to 0.16% (**Figure 5a**) is associated with enrichment of the passive layer with carbide and oxide products (**Table 4**). Al is a very reactive element and has a high affinity for oxygen so forming AlO during the corrosive attack [28]. In addition, the FeAlC and AlC intermetallic compounds dissolve during immersion, so resulting in carbide and oxide, which diffuse on the surface, so slowing down any further attack by obstructing the current flow [41,42], (**Figure 5a**), and restricting the severe pitting attack (**Figure 4b**). The volume fraction of FeAlC, AlC and AlO is expected to increase with increasing Al content, so further enrichment of the passive layer is attained, (**Table 4**). The addition of Nb provided an additional benefit by promoting passivation behaviour (**Figure 5a**). Nb has a high affinity to C, so the steel is rich with NbC compounds, which contributed markedly to slowing down the current flow, (**Figure 5a**), so minimising pitting corrosion (**Figure 4c**). This observation agrees with a recent study by Amaya et al. [43], which concluded that NbC is effective in promoting corrosion resistance of gray iron against palm biodiesel. The formation of NbO provided an additional benefit (**Table 4**), and previous work reported the use of NbO as a biomedical coating, which proved to be sufficient to provide protection to the stainless steel substrate [44].

4. Conclusions

The effect of Al and Nb contents, cooling rate and rolling condition on the corrosion behaviour of HSLA steel in 10 wt% sulphuric acid has been investigated, and the following conclusions can be drawn.

- (1) Increasing the Al content from 0.02 to 0.16% in the HSLA steel improved the corrosion resistance by obstructing pitting attack due to the refinement of the density and thickness of the grain boundary carbides, and enrichment of the passive layer with carbide and oxide products.
- (2) In the presence of Nb, the grain size was refined, martensite was formed while the thickness and volume fraction of grain boundary carbides increased. The induced microstructural features were considered detrimental to corrosion behaviour but the combination of both Al and Nb contributed to the enrichment of the passive film on the surface with Nb and higher levels of carbide and oxide products that promoted the corrosion resistance.
- (3) Increasing the cooling rate refined the grain size and reduced the thickness of grain boundary carbides. The latter being beneficial but the former is detrimental and more dominant due to the availability of higher density of boundaries, which act as active sites for corrosion and also increases the density of distributed carbides. Both factors contributed to accelerate the dissolution rate of the steel in the corrosive electrolyte.
- (4) Controlled rolling provides better corrosion resistance because of the absence of martensite, the finer grain boundary carbides and the lower angle boundary in comparison with the hot rolling process.

Acknowledgment

The authors would like to thank Tata Steel in the UK for supplying the steel samples.

Data Availability statement

The raw/processed data required to reproduce these findings cannot be shared at this time as the data also forms part of an ongoing study.

References:

1. Konstruksijska, V.M.H., 2011. High-strength low-alloy (HSLA) steels. *Materiali in tehnologije*, 45(4), pp.295-301.
2. Qaban, A., 2019. *The effect of alloying composition and cooling rate on the hot ductility of TWIP steel and mechanical properties of hot rolled HSLA steel* (Doctoral dissertation, City University London).
3. Stowe Jr, D.H. and Blakefield, W.S., Omni Materials Inc, 2008. *Method for reducing the amount of a sulfur dioxide in a flue gas resulting from the combustion of a fossil fuel*. U.S. Patent 7,430,969.
4. McDonald, D.K. and Rogers, K.J., Babcock and Wilcox Power Generation Group Inc, 2014. *Segregated in-situ forced oxidation wet flue gas desulfurization for oxygen-fired fossil fuel combustion*. U.S. Patent 8,795,416.
5. Lu, B.T., Luo, J.L. and Norton, P.R., 2010. Environmentally assisted cracking mechanism of pipeline steel in near-neutral pH groundwater. *Corrosion science*, 52(5), pp.1787-1795.
6. Quazi, M.M., Ishak, M., Fazal, M.A., Arslan, A., Rubaiee, S., Qaban, A., Aiman, M.H., Sultan, T., Ali, M.M. and Manladan, S.M., 2020. Current research and development status of dissimilar materials laser welding of titanium and its alloys. *Optics & Laser Technology*, 126, p.106090.
7. Quazi, M.M., Ishak, M., Fazal, M.A., Arslan, A., Rubaiee, S., Aiman, M.H., Qaban, A., Yusof, F., Sultan, T., Ali, M.M. and Manladan, S.M., 2020. A comprehensive assessment of laser welding of biomedical devices and implant materials: recent research, development and applications. *Critical Reviews in Solid State and Materials Sciences*, pp.1-43.
8. Mintz, B., Qaban, A., Bendke, P. and Naher, S., 2020. The influence of a high aluminium addition on the strength and impact behaviour of hot-rolled Nb containing steels. *Materials Science and Technology*, 36(2), pp.233-244.
9. Mintz, B., Qaban, A. and Naher, S., 2020. Further insights on compositional control and heat treatment for improving the impact behaviour of hot-rolled steels containing Nb and Al. *Materials and Design*, 190, p.108601.
10. Qaban, A., Mintz, B. and Naher, S., 2017. Hot rolled high Al containing steels as a replacement for the control rolled high strength low alloy (HSLA) steels. In *AIP Conference Proceedings* (Vol. 1896, No. 1, p. 130007). AIP Publishing.
11. Qaban, A., Mintz, B., Kang, S.E. and Naher, S., 2017. Hot ductility of high Al TWIP steels containing Nb and Nb-V. *Materials Science and Technology*, 33(14), pp.1645-1656.
12. Qaban, A., 2019. *The effect of alloying composition and cooling rate on the hot ductility of TWIP steel and mechanical properties of hot rolled HSLA steel* (Doctoral dissertation, City, University of London).
13. Jung, J.G., Park, J.S., Kim, J. and Lee, Y.K., 2011. Carbide precipitation kinetics in austenite of a Nb-Ti-V microalloyed steel. *Materials Science and Engineering: A*, 528(16-17), pp.5529-5535.
14. Song, F., Zhang, S. and Zhang, K., 2017. Influence of Aluminum Addition on the Corrosion of 304 Stainless Steel in High Temperature Water. *J Nucl Ene Sci Power Generat Technol* 6, 4, p.2.
15. Andrianingtyas, R.M., Anwar, M.S., Hastuty, S., Widharyanti, I.D., Dahliyanti, A., Prastomo, N. and Mabururi, E., 2018, May. Role of tungsten, niobium, and vanadium on

- corrosion resistance of austenitic stainless steels in chloride ion environment. In *AIP Conference Proceedings* (Vol. 1964, No. 1, p. 020034). AIP Publishing LLC.
16. Chen, Y.T. and Zhang, K.G., 2012. Influence of grain size on corrosion resistance of a HSLA steel. In *Advanced Materials Research* (Vol. 557, pp. 143-146). Trans Tech Publications Ltd.
 17. Hadzima, B., Janeček, M., Estrin, Y. and Kim, H.S., 2007. Microstructure and corrosion properties of ultrafine-grained interstitial free steel. *Materials Science and Engineering: A*, 462(1-2), pp.243-247.
 18. Li, Y., Wang, F. and Liu, G., 2004. Grain size effect on the electrochemical corrosion behavior of surface nanocrystallized low-carbon steel. *Corrosion*, 60(10), pp.891-896.
 19. Mintz, B., Tajik, S. and Vipond, R., 1994. Influence of microalloying additions on thickness of grain boundary carbides in ferrite–pearlite steels. *Materials science and technology*, 10(2), pp.89-96.
 20. ASTM Standard G 31-72, Standard practice for laboratory immersion corrosion testing of metals (American Society for Testing and Materials, 2004), pp. 1-8
 21. Bayoumi, F.M. and Ghanem, W.A., 2005. Effect of nitrogen on the corrosion behavior of austenitic stainless steel in chloride solutions. *Materials Letters*, 59(26), pp.3311-3314.
 22. Qaban, A. and Naher, S., 2019. Investigation of corrosion resistance of high-strength low-alloy (HSLA) steel in fresh and salt water for pipeline application. In *AIP Conference Proceedings* (Vol. 2146, No. 1, p. 020021). AIP Publishing.
 23. Mintz, B., 2003. The influence of Al on the mechanical properties of hot rolled steel plates. In *Materials Science Forum* (Vol. 426, pp. 1219-1223). Trans Tech Publications Ltd., Zurich-Uetikon, Switzerland.
 24. Mintz, B., Gunawardana, W.D. and Su, H., 2008. Al as solid solution hardener in steels. *Materials Science and Technology*, 24(5), pp.596-600.
 25. Soleimani, M., Mirzadeh, H. and Dehghanian, C., 2019. Processing route effects on the mechanical and corrosion properties of dual phase steel. *Metals and Materials International*, pp.1-9.
 26. Salamci, E., Candan, S. and Kabakci, F., 2017. Effect of microstructure on corrosion behavior of dual-phase steels. *Kovove Mater*, 55, pp.133-139.
 27. Wilmes, S. and Zwick, G., 2002. Effect of niobium and vanadium as an alloying element in tool steels with high chromium content. *The Use of Tool Steels: Experience and Re-search*, 1, pp.227-243.
 28. Olasolo, M., Uranga, P., Rodriguez-Ibabe, J.M. and López, B., 2011. Effect of austenite microstructure and cooling rate on transformation characteristics in a low carbon Nb–V microalloyed steel. *Materials Science and Engineering: A*, 528(6), pp.2559-2569.
 29. KA, A. and HJ, K., 2007. The influence of niobium microalloying on austenite grain coarsening behavior of Ti-modified SAE 8620 steel. *ISIJ international*, 47(2), pp.307-316.
 30. Wei, S. and Lu, S., 2012. Effects of multiple normalizing processes on the microstructure and mechanical properties of low carbon steel weld metal with and without Nb. *Materials & Design*, 35, pp.43-54.
 31. Soleimani, M., Mirzadeh, H. and Dehghanian, C., 2020. Effect of grain size on the corrosion resistance of low carbon steel. *Materials Research Express*, 7(1), p.016522.
 32. Mosayebi, M., Zarei-Hanzaki, A., Abedi, H.R., Barabi, A., Jalali, M.S., Ghaderi, A. and Barnett, M., 2020. The correlation between the recrystallization texture and subsequent isothermal grain growth in a friction stir processed rare earth containing magnesium alloy. *Materials Characterization*, p.110236.

33. Barabi, A., Zarei-Hanzaki, A., Abedi, H., Anoushe, A. and Cho, J.H., 2018. The Correlation of Macrostructure, Microstructure, and Texture with Room Temperature Mechanical Properties of a Twinning-Induced Plasticity Automotive Steel after Friction Stir Spot Welding/Processing. *steel research international*, 89(11), p.1800245.
34. Howe, A.A., 2000. Ultrafine grained steels: industrial prospects. *Materials Science and Technology*, 16(11-12), pp.1264-1266.
35. Li, Y., Wang, F. and Liu, G., 2004. Grain size effect on the electrochemical corrosion behavior of surface nanocrystallized low-carbon steel. *Corrosion*, 60(10), pp.891-896.
36. Coll Ferrari, M.T., 2015. *Effect of austenitising temperature and cooling rate on microstructures of hot-work tool steels* (Doctoral dissertation, University West).
37. Ismail, M., Muhammad, B., Hamzah, E. and Keong, T., 2012. Corrosion behaviour of dual-phase and galvanized steels in concrete. *Anti-Corrosion Methods and Materials*, 59(3), pp.132-138.
38. Nadlene, R., Esah, H., Norliana, S. and Irwan, M.M., 2011. Study on the effect of volume fraction of dual phase steel to corrosion behaviour and hardness. *World Academy of Science, Engineering and Technology*, 5(2), pp.564-567.
39. Keleştemur, O., Aksoy, M. and Yildiz, S., 2009. Corrosion behavior of tempered dual-phase steel embedded in concrete. *International Journal of Minerals, Metallurgy and Materials*, 16(1), pp.43-50.
40. Yuan, X., Zhao, Y., Li, X. and Chen, L., 2017. Effect of Cr on mechanical properties and corrosion behaviors of Fe-Mn-C-Al-Cr-N TWIP steels. *Journal of Materials Science & Technology*, 33(12), pp.1555-1560.
41. Wang, H.Z., Leung, D.Y., Leung, M.K.H. and Ni, M., 2009. A review on hydrogen production using aluminum and aluminum alloys. *Renewable and sustainable energy reviews*, 13(4), pp.845-853.
42. Liao, X. and Øye, H.A., 2016. Carbon cathode corrosion by aluminium carbide formation in cryolitic melts. In *Essential Readings in Light Metals* (pp. 992-998). Springer, Cham.
43. Amaya, A., Piamba, O. and Olaya, J., 2018. Improvement of corrosion resistance for gray cast iron in palm biodiesel application using thermoreactive diffusion niobium carbide (NbC) coating. *Coatings*, 8(6), p.216.
44. Rojas, P.N. and Rodil, S.E., 2012. Corrosion behaviour of amorphous niobium oxide coatings. *Int J Electrochem Sci*, 7, pp.1443-1458.